



^{1,2} Cornel SUCIU, ² Ionuț Cristian ROMĂNU, ³ Tiberiu Ștefan MĂNESCU,
⁴ Răzvan AVRAM, ⁵ Cristian-Marius MIMIS

MODELING OF HYPER-ELASTIC MATERIALS IN CONTACT

^{1,2} Ștefan cel Mare University of Suceava, ROMANIA

³⁻⁵ Eftimie Murgu University, Reșița, ROMANIA

Abstract: Current technology in machine and equipment industry frequently employs components made from hyper-elastic materials such as rubber, various polymeric foams etc. When pressed against another body, such materials illustrate different behavior by comparison to the contacts of linear elastic materials. It is therefore of interest to investigate the mechanical behavior of such materials in contact. The present paper advances a finite element model of the circular contact between a spherical punch made from a hyper-elastic material and a rigid half-space. The numerically obtained results are then compared to previously advance experimental results.

Keywords: rubber, hyper-elastic behavior, simulation, circular contact

INTRODUCTION

As the practical situations are extremely different, numerous studies can be found in literature, [1-8] that investigate, either theoretically or experimentally, the behavior of bodies pressed against each other under different conditions.

The literature of the last half-century contains various models for hyper-elastic behavior of materials, [1-5].

Rivlin and Mooney advanced such a model, [1-4] that was found to be suitable for investigations upon the behavior of rubber and other similar materials.

The present paper advances a finite element model of the circular contact between a spherical punch made from a hyper-elastic material and a rigid half-space.

HYPER-ELASTIC MATERIAL MODELING

Most of the models currently employed for the characterization of materials with nonlinear elastic behavior are based upon specific strain energy expressions, [1]. The most commonly used model that characterizes hyper-elastic materials is the generalized Rivlin model. The general equation for specific strain energy is according to [2], as follows:

$$W = \sum_{p,q=0}^N C_{pq} (\bar{I}_1 - 3)^p (\bar{I}_2 - 3)^q + \sum_{m=1}^M D_m (J - 1)^{2m}, \quad (1)$$

where, C_{pq} represent material constants that depend on shape modifications of the investigated material and D_m are material constants that depend on volume variations. In the case of compressible materials, $N = 1$, $M = 1$, $C_{00} = C_{11} = 0$, and W becomes:

$$W = C_{01} (\bar{I}_2 - 3) + C_{10} (\bar{I}_1 - 3) + D_1 (J - 1)^2, \quad (2)$$

where, $\bar{I}_1 = J^{-2/3} I_1$, $I_1 = \lambda_1^2 + \lambda_2^2 + \lambda_3^2$, $J = \det(\hat{F})$, $\bar{I}_2 = J^{-4/3} I_2$, thus resulting that $I_2 = \lambda_1^2 \lambda_2^2 + \lambda_2^2 \lambda_3^2 + \lambda_3^2 \lambda_1^2$. In the case of incompressible materials, equation (2) is rewritten as:

$$W = C_1 (\lambda_1^2 + \lambda_2^2 + \lambda_3^2 - 3) + C_2 (\lambda_1^2 \lambda_2^2 + \lambda_2^2 \lambda_3^2 + \lambda_3^2 \lambda_1^2 - 3). \quad (3)$$

Due to material incompressibility, $C_{01} = C_2$, $C_{10} = C_1$, and $\lambda_1 \lambda_2 \lambda_3 = 1$, while the term that characterizes volume strains annuls. Mooney, according to [3], defines nonlinear elastic behavior of materials by aid of an expression similar to the one given in equation (4). The material constants C_1 and C_2 employed by this model can be determined from the stress – uniaxial strain under traction, Figure 1, with the assumption that the material is incompressible, homogenous and isotropic, as showed in [3]. The model advanced by Mooney is a particular case of the generalized Rivlin model for incompressible materials. The specific strain energy is defined by aid of two invariants of the Cauchy – Green strain tensor.

$$W = C_1 (\bar{I}_1 - 3) + C_2 (\bar{I}_2 - 3), \quad (4)$$

where, C_1 and C_2 are material constants, \bar{I}_1 and \bar{I}_2 represent the first and second invariants of the Cauchy – Green strain tensor, respectively. Literature, [2], presents rubber as being an incompressible material and having a transverse contraction coefficient value in the vicinity of 0.5.

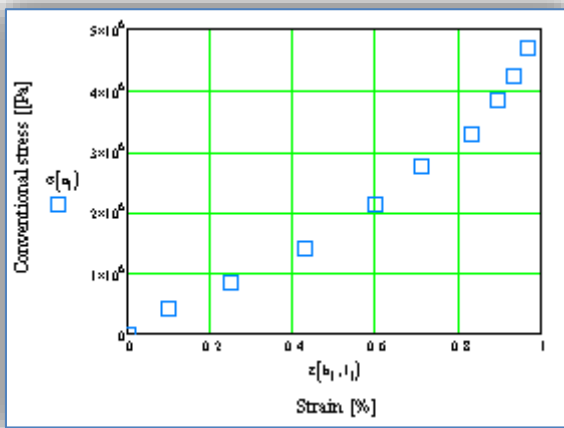


Figure 1: Stress – strain characteristic for rubber, experimentally obtained under uniaxial traction, [4, 5].

For incompressible materials with hyper-elastic behavior, Vossoughi, [3] advanced a representation of the specific strain energy as follows:

$$W = C_1 \left(\lambda^2 + \frac{2}{\lambda} - 3 \right) + C_2 \left(2\lambda + \frac{1}{\lambda^2} - 3 \right), \quad (5)$$

where, constants C_1 and C_2 are obtained by derivation of the specific strain energy by report to the two invariants of the Cauchy – Green strain tensor, \bar{I}_1 and \bar{I}_2 , respectively, as shown in [3]. By derivation of equation (5) by report to λ , it results that, [3]:

$$\sigma = \frac{\partial W}{\partial \lambda} = 2C_1 \left(\lambda - \frac{1}{\lambda^2} \right) + 2C_2 \left(1 - \frac{1}{\lambda^3} \right). \quad (6)$$

In order to obtain a linearization of the characteristic, equation (6) can be rewritten as:

$$\frac{\sigma}{2(\lambda - \lambda^{-2})} = C_1 + \frac{1 - \lambda^{-3}}{\lambda - \lambda^{-2}} C_2. \quad (7)$$

If it is considered that $Y = \frac{\sigma}{2(\lambda - \lambda^{-2})}$ and $X = \frac{1 - \lambda^{-3}}{\lambda - \lambda^{-2}}$,

equation (7) can be rewritten as shown in, [3], as:

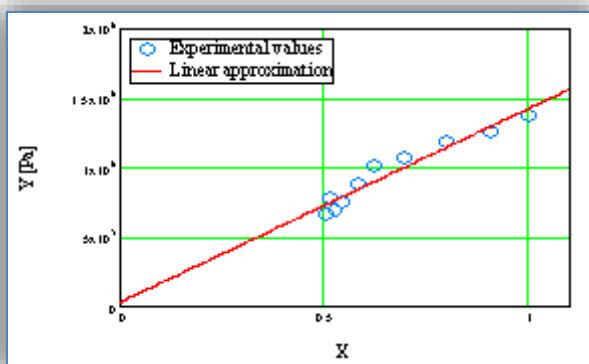
$$Y = C_1 + C_2 \cdot X. \quad (8)$$


Figure 2: Y – X characteristic for rubber, obtained under uniaxial traction.

By graphically representing Y as a function of X, a linear plot is obtained as shown in Figure 2. The slope and intersection with the ordinate axis of this plot represent the values of C_2 and C_1 constants, respectively, [4].

Using a calculus methodology previously described in [3], the following material constants were obtained for the investigated rubber: $C_1 = 33,9 \text{ kPa}$, and $C_2 = 1,395 \text{ MPa}$. The obtained material constants were then used as input data in finite element analysis (FEA) software, in order to model the nonlinear elastic behavior of materials.

MODELING OF HYPER-ELASTIC SPHERICAL BODY – RIGID HALF-SPACE CONTACT

For the present study, a contact between a hyper-elastic spherical punch and a rigid half-space was modeled using the FEA software Femap.

In order to reduce the necessary time for calculus in such a model, only a 10° sector of a hemisphere was modeled from the total punch volume, as illustrated in Figure 3.

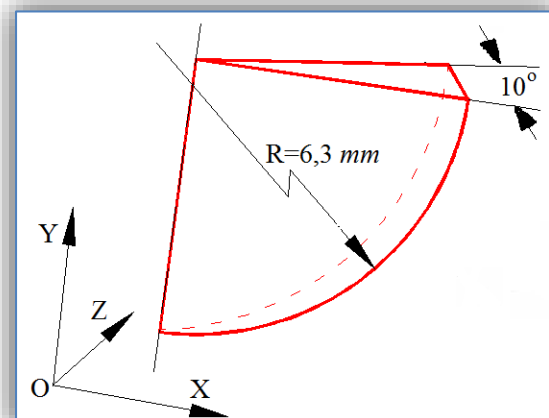


Figure 3: Geometry of the hemisphere sector created to model the 12.6mm rubber ball.

This simplification of the geometry was possible as it was taken into account that such a contact presents axial symmetry. The present study was conducted considering a rubber ball with a diameter of 12.6 mm.

As previously stated, it was considered that the punch is a ball made from rubber. Material elastic properties are defined by aid of the material constants from the Mooney-Rivlin model. For the present study, the material constants taken into consideration were $C_1 = 33,9 \text{ kPa}$, and $C_2 = 1,395 \text{ MPa}$, as previously described.

For the generation of finite elements in the described model, an automatic meshing was employed. Hexahedral elements of variable dimensions were placed on the considered geometry as follows: 40 elements unevenly placed over the length of the

circle arc, 30 elements evenly placed along the hemisphere symmetry axis and 20 elements evenly placed along a radius considered perpendicular to the symmetry axis.

The node corresponding to the initial point of contact between the rubber sphere and the rigid half-space was fixed (all degrees of freedom were removed). The displacements of nodes corresponding to the two lateral faces are restricted to their respective planes. Nodes placed on the symmetry axis can only move along the vertical axis, Y. The nodes corresponding to the upper surface of the geometry are allowed to have displacements along radial directions and also along the Y axis.

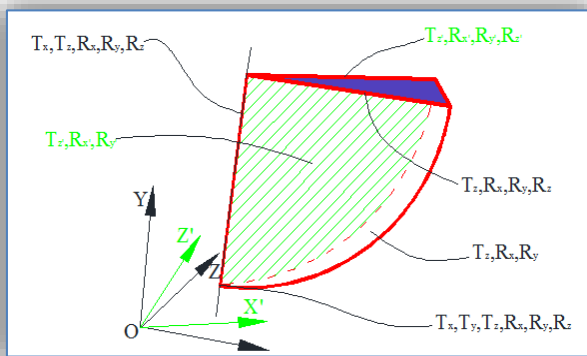


Figure 4: Constraints applied to the various geometry elements

In the representation of the constrained geometry illustrated by Figure 4, $T_x, T_y, T_z, T_{x'}, T_{y'}, T_{z'}$ denote the translations constrained (not allowed) along the X, Y, Z, X', Y', Z' directions, while $R_x, R_y, R_z, R_{x'}, R_{y'}, R_{z'}$ represent the constrained rotations around the X, Y, Z, X', Y', Z' directions.

The contact is loaded by means of imposed displacements of the nodes from the upper plane of the considered hemisphere sector.

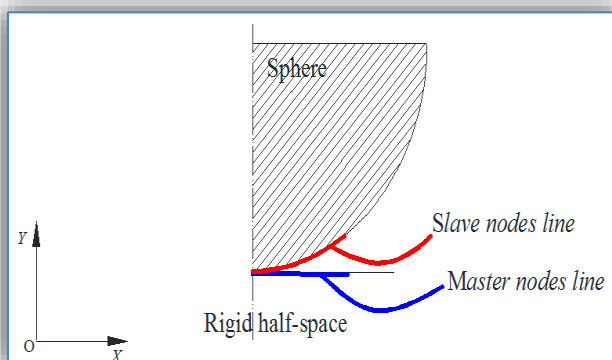


Figure 5. Nodes corresponding to the master and slave sliding lines.

For the present contact model, the creation of two sliding lines was necessary. These were defined by selection of corresponding nodes from the two

geometries of contacting bodies. Slave sliding lines were defined on the ball geometry, while master lines were defined using the half-space geometry, as illustrated by Figure 5.

The presented contact model was analyzed using a static-nonlinear analysis that uses 30 steps.

RESULTS AND DISCUSSIONS

After the simulations were conducted as described above, the obtained results were represented graphically and interpreted. Figure 7 illustrates a spatial distribution of σ_y stresses corresponding to the considered hemisphere sector.

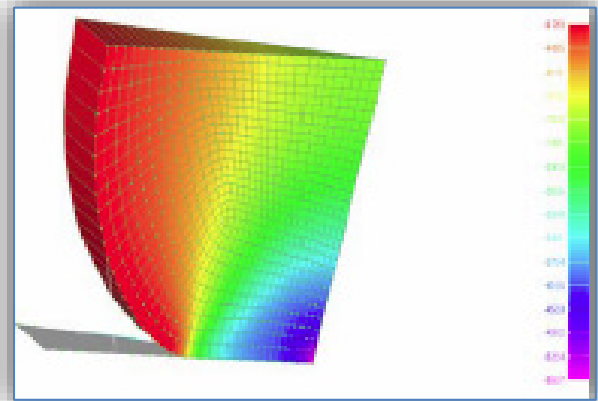


Figure 6: σ_y stress distribution corresponding to an imposed normal approach of 1,42 mm, for the contact between a rubber ball with $D = 12,6 \text{ mm}$ and a rigid half-space.

From the stress distribution plot illustrated in Figure 6, it can be noticed that the σ_y stresses take negative values in the contact region and become positive outside it. Also, as expected, it can be observed that the absolute values of these stresses are more important in nodes placed inside the contact region than in the ones outside it.

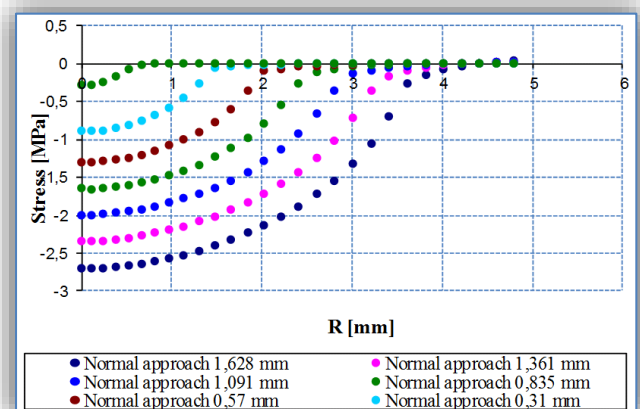


Figure 7: σ_y stress distribution along radial direction, corresponding to several imposed normal approach values, for the contact model between a $D = 12,6 \text{ mm}$ - rubber ball and a rigid half-space.

In order to evaluate the σ_y stress radial distribution, the values corresponding to nodes placed on one of the two circular contours limiting the hemisphere sector were represented graphically. Figure 7 illustrates such stress distribution plots, corresponding to various imposed displacements. In order to assess whether the σ_y stress distribution obtained in this study is similar to the one yielded by the Hertz model for point contacts, several σ_y stress values were selected and interpolated by a function given by: $p(x) = p_0 \sqrt{1 - \frac{x^2}{r^2}}$.

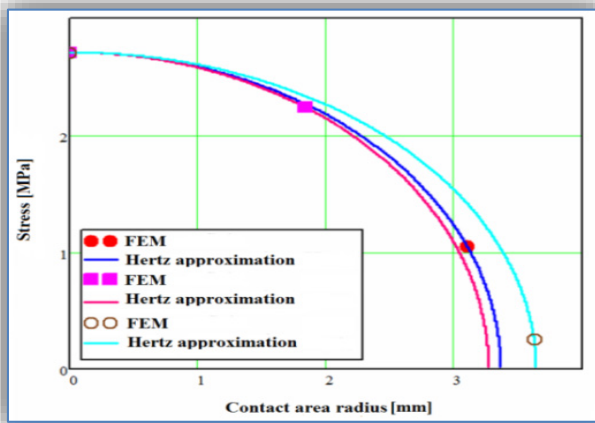


Figure 8: Interpolation of the FEA results for comparison to Hertz contact model.

The graphical representation of stress radial distribution illustrated in Figure 8 show that the three plots do not coincide. If the σ_y stress distribution in the investigated contact model were similar to a Hertz distribution, the three plots would overlap. It can therefore be stated that the stress distribution in the case of a circular contact between nonlinear elastic materials is different from the one yielded by Hertz theory.

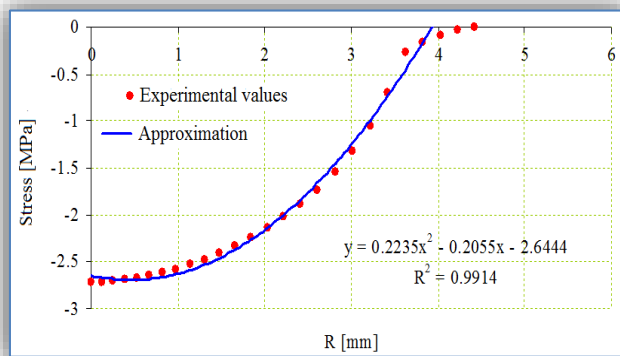


Figure 9: σ_y stress distribution corresponding to an imposed normal approach of 1.628 mm, for the contact model between a $D = 12,6$ mm - rubber ball and a rigid half-space.

Figure 9 illustrates the σ_y stress distribution corresponding to an imposed normal displacement of 1.628 mm.

The presented finite element model and conducted analysis allows the assessment of the approximate value of the contact area radius at the intersection of the interpolation curve illustrated in Figure 9 and the X-axis.

Using this method, contact area radii were determined at various imposed normal displacements and their evolution was plotted as shown in Figure 10.

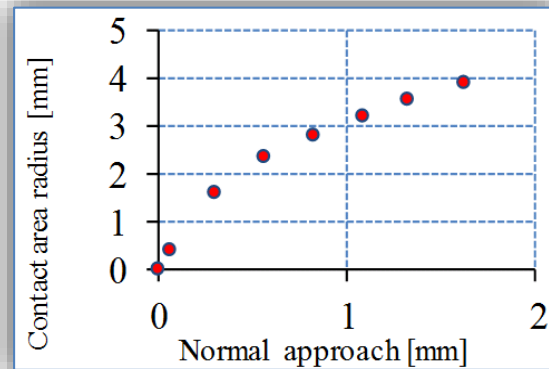


Figure 10: Correlation between contact area radius and normal approach for the contact model between a $D = 12.6$ mm - rubber ball and a rigid half-space.

The plot illustrated in Figure 10 shows a nonlinear evolution of the contact area dimensions as the imposed normal approach increases. The shape of the numerically obtained stress evolution plot is similar to previously advanced experimental results. Further analysis of the σ_y stress distributions shown in Figure 8 illustrate that maximum stresses are reached in the center of the contact area. Figure 11 graphically illustrates the evolution of these maximum stresses as normal approach increases.

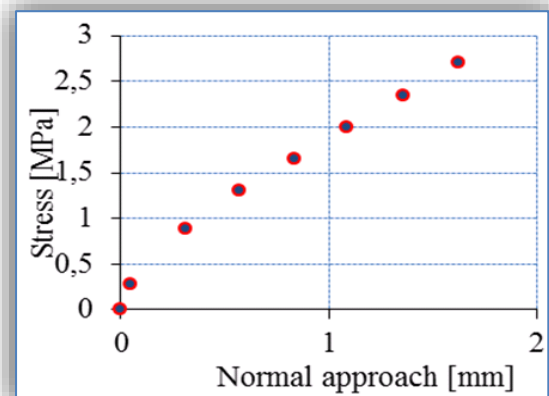


Figure 11. Correlation between maximum stress value and normal approach for the contact model between a $D = 12.6$ mm - rubber ball and a rigid half-space.

The numerical results yielded by this model were compared to experimental investigations conducted on the circular contact between a rubber sphere with a diameter $D = 12.6\text{mm}$, compressed between the flat surfaces of two parallel optically transparent sapphire plates. By report to the rubber ball, the two diametrically opposed plates can be assimilated to rigid half-spaces, as previously described in [5]. This experimental setup and methodology, as described in [5], generates two rubber ball – flat rigid surface, identical contacts (top and bottom), one of which is investigated.

The obtained contact area was investigated optically and its dimensions were determined. For that purpose the contact area was visualized and photographed by aid of an optical microscope. The obtained images of the contact area were then analyzed and its dimensions were determined by comparison to a sample with known size (1.34mm), as shown in Figure 12.

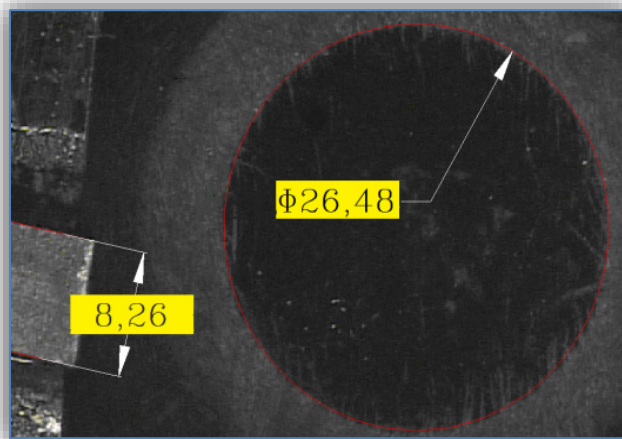


Figure 12: Contact area for an applied load of 13.05N, corresponding to a normal approach of 0.64mm

The normal approach between the two sapphire plates, which gives the rubber ball deformation along the vertical axis, was determined by aid of a laser profilometer.

The laser beam from the optical sensor of the profilometer was focused on the same sapphire surface before and after application of normal load to the contact. The difference between the two focus points, yields the total deformation of the rubber ball along the vertical axis.

The measured value represents double the value of the normal approach corresponding to one of the two rubber ball rigid surface contacts.

The correlation between experimental results obtained as described above and numerical simulations yielded by FEM analysis is shown in Figure 13.

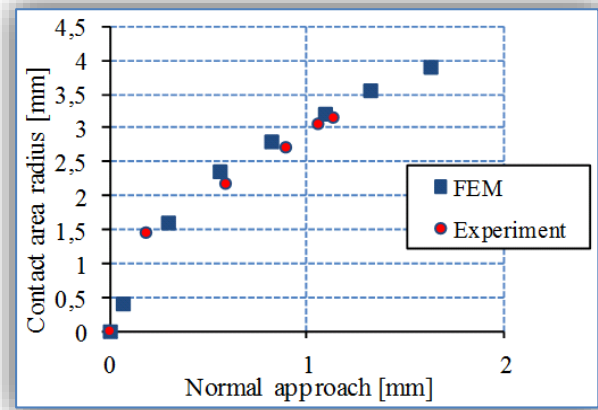


Figure 13: Comparison between the contact area radii obtained experimentally and FEM simulations, for the contact model between a $D = 12,6\text{mm}$ rubber ball and a rigid half-space.

CONCLUSIONS

In order to simulate the behavior of a hyper-elastic, homogenous isotropic and incompressible material using a Mooney-Rivlin model, it is necessary to determine the corresponding material constants. This can be accomplished by conducting a uniaxial traction test on the investigated material and following the procedure previously described in [3] and [4].

In order to simulate a circular contact between bodies with hyper-elastic behavior it was found to be sufficient to model only a part of the total punch volume. In the present paper, a 10° sector of a hemisphere was considered for the modeling of a ball pressed against a flat rigid surface. The good agreement found between numerical simulations and experimental results confirm this possibility.

The normal stress distribution found in the case of hyper-elastic bodies in contact was found to be different from the one yielded by a Hertz model of a circular contact, which considers elastic behavior.

Note

This paper is based on the paper presented at The 1st International Conference "Experimental Mechanics in Engineering" - EMECH 2016, organized by Romanian Academy of Technical Sciences, Transilvania University of Brasov and Romanian Society of Theoretical and Applied Mechanics, in Brasov, ROMANIA, between 8 - 9 June 2016

References

- [1.] OGDEN, R., W., Non-linear elastic deformations, ISBN 0-486-69648-0, 1997.
- [2.] RIVLIN, R., SAUNDERS, D., W., Large elastic deformations of isotropic materials vii. Experiments on the deformation of rubber, Phi. Trans. Royal Soc. London Series A, 243(865), pp. 251-288, 1951.
- [3.] VOSSOUGH, J., Determination of Mooney material constants for highly nonlinear isotropic

- incompressible materials under large elastic deformations, 1995.
- [4.] ROMÂNU I. C. Experimental method used to determine Mooney - Rivlin constants for rubber. Part I, TEHNOMUS Journal, pp34-39, ISSN 2247-6016.
 - [5.] ROMÂNU I. C. Experimental method used to determine Mooney - Rivlin constants for rubber. Part II, TEHNOMUS Journal, pp. 468-471, ISSN 2247-6016.
 - [6.] ROMÂNU I. C. The End Effect in Finite Line Length Contact Between Nonlinear Elastic Bodies, PhD Thesis, Suceava, 2013
 - [7.] MANESCU, T., JR.; GILICH, G.-R.; MANESCU, T.S.; SUCIU, C., Optical Evaluation of Surface Defects Influence upon the Contact Area between a Metallic Spherical Punch and a Flat Surface, MATERIALE PLASTICE Volume: 51 Issue: 2 Pages: 157-161, 2014
 - [8.] MĂNESCU TIBERIU JR., GILICH GILBERT-RAINER, MĂNESCU TIBERIU ȘTEFAN, SUCIU CORNEL, 2013, Experimental Investigations upon Contact Behavior of Ball Bearing Balls Pressed Against Flat Surfaces, Proceedings of COMEC 2013, ISBN-10: 1939757118, ISBN-13: 978-1939757111



ACTA Technica CORVINIENSIS
BULLETIN OF ENGINEERING

ISSN:2067-3809

copyright ©
University POLITEHNICA Timisoara,
Faculty of Engineering Hunedoara,
5, Revolutiei, 331128, Hunedoara, ROMANIA
<http://acta.fih.upt.ro>